Cloud ~~droplet~~ activation properties of aerosol particles
in a continental central European urban environment

Imre SALMA[1], Wanda THÉN[2], Máté VÖRÖSMARTY[2], and András Zénó GYÖNGYÖSI[1]

[1] Institute of Chemistry, Eötvös Loránd University, Budapest, Hungary
[2] Hevesy György Ph. D. School of Chemistry, Eötvös Loránd University, Budapest, Hungary

Correspondence to: Imre Salma (salma.imre@ttk.elte.hu)

Abstract. Collocated measurements by condensation particle counter, differential mobility particle sizer and cloud condensational nuclei counter instruments were realised in parallel in central Budapest from 15 April 2019 to 14 April 2020 to gain insight into the ~~droplet~~ cloud activation ~~behaviour~~ properties of urban aerosol particles. The median total particle number concentration was 10.1×10^3 cm^{-3}. The median concentrations of cloud condensation nuclei (CCN) at water vapour supersaturations (Ss) of 0.1, 0.2, 0.3, 0.5 and 1.0 % were 0.59, 1.09, 1.39, 1.80 and 2.5×10^3 cm^{-3}, respectively. They represented from 7 to 27 % of the total particles. The CCN concentrations were considerably larger, whereas the activation fractions were substantially and systematically smaller than for regional or remote locations. The effective critical dry particle diameters ($d_{c,eff}$) were derived utilising the CCN concentrations and particle number size distributions. Their medians were 207, 149, 126, 105 and 80 nm, respectively. They were positioned within the accumulation mode of the typical particle number size distribution. Their frequency distributions revealed a single peak, which geometric standard deviation increased monotonically with S. The broadening indicated large time variability in the activation properties of smaller particles. The frequency distributions also showed a fine structure. Its several compositional elements seemed to change in a tendentious manner with S. ~~They were related to the size-dependent chemical composition and external mixtures of particles.~~ The relationships between the critical S and $d_{c,eff}$ suggested that the urban aerosol particles in Budapest with a diameter larger than approximately 130 nm showed similar hygroscopicity than the continental aerosol in general, whereas the smaller particles were less hygroscopic than that. Seasonal cycling of the CCN concentrations and activation fractions implied modest alterations and for the larger Ss only. They likely reflected the changes in particle number concentrations, chemical composition and mixing state of particles as well. The seasonal dependencies for $d_{c,eff}$ were featureless, which indicated that the urban particles exhibited more or less similar droplet activation properties over the year. This is again different from non-urban locations. The hygroscopicity parameters (κ values) were computed without determining time-dependent chemical composition of particles. Their medians were 0.15, 0.10, 0.07, 0.04 and 0.02, respectively. The averages suggested that the larger particles exhibited considerably higher hygroscopicity than the smaller particles. We found that the ~~The~~ urban aerosol ~~was characterised by~~ showed substantially smaller κ values than for regional or remote locations, which were reported previously. All these could be virtually linked to specific source composition of particles in cities. The relatively large variability in the hygroscopicity parameter sets for a given S emphasized that

their individual values represented the CCN population in the ambient air, while the averages stood mainly for the particles with a size close to the effective critical dry particle diameters.

1 Introduction and objectives

Water is the most abundant vapour in the troposphere. Its condensation onto aerosol particles is the only relevant pathway for cloud or fog droplet formation at water vapour supersaturations (Ss) occurring in the ambient air (Pruppacher and Klett, 2000). The Ss in clouds are usually less than 1 % with a median value between 0.1 and 0.2 %. The number and size of the generated droplets depend both on particle properties and actual local S (Andreae and Rosenfeld, 2008). Only a subset of aerosol particles are able to grow to droplets at a given S; they are called cloud condensation nuclei (CCN) for this S. From the aerosol side, this ability is primarily controlled by the size of particles and to a lesser degree by , their chemical composition and mixing state of particles (Dusek et al., 2006). The Ss are mainly governed by cloud dynamics and also by existing cloud droplets. The latter property acts as a sink of water vapour and depends on CCN concentrations as well. Different updraft velocities and droplet populations in clouds result in different Ss, which can also change the activation process. As a consequence, the droplet formation can be limited by the availability of CCN and/or updraft velocities. The former case ordinarily prevails in the global troposphere at concentrations of $<9\times10^3$ cm^{-3} and is called CCN-limited regime (Rosenfeld et al., 2014).

The CCN modify the intensity and other properties of the sunlight reaching the Earth's surface indirectly through cloud droplets. It is achieved primarily through the droplet number, droplet size and cloud residence time (Andreae and Rosenfeld, 2008; Rosenfeld et al., 2008, 2014). They also influence the hydrological cycle including the precipitation amount and intensity, the vegetation and its interactions with the carbon cycle as well as the atmospheric chemistry, physics and dynamics. Moreover, it is this indirect effect of aerosols that has the most uncertain contribution to the global radiative forcing calculations (e.g. Carslaw et al., 2013). This is particularly important since the number concentrations of particles seem to be increasing globally due to anthropogenic activities (Andreae et al., 2005). Concentrations of CCN can vary considerably in space and time. Dedicated studies have been performed in field experiments at several locations in the world and at various laboratories (e.g. Dusek et al., 2006; McFiggans et al., 2006; Hudson, 2007; Rose et al., 2008, 2010; Kuwata and Kondo, 2008; Pringle et al., 2010; Wex et al., 2010; Burkart et al., 2011; Sihto et al., 2011; Jurányi et al., 2011; Kerminen et al., 2012; Topping and McFiggans, 2012; Paramonov et al., 2015; Herenz et al., 2018; Schmale et al., 2018). Despite their importance, our knowledge on aerosol–water vapour interactions at supersaturations typical for in the atmospherice under supersaturated conditions and on cloud microphysics have remained still insufficient. Longer-term studies (for instance, of at least 1 full year) are preferredrequired to understand

70 these processes and their consequences. A broad regional coverage is also desired to reach representative

71 results. The data sets for the environmental category of large cities are particularly scarce.

72

73 The study presented here deals with the cloud droplet activation properties of aerosol particles in a

74 continental central European city, Budapest. It has 2.2 million inhabitants in the metropolitan area, and it

75 is the largest city in the Carpathian Basin. Online aerosol and meteorological measurements have been

76 going on in a semi-continuous manner at the Budapest platform for Aerosol Research and Training

77 (BpART) Laboratory for more than a decennium (Salma et al., 2011; Mikkonen et al., 2020). The related

78 essential instruments include a differential mobility particle sizer (DMPS) and a condensation particle

79 counter (CPC). They were complemented by a continuous-flow cloud condensation nuclei counter

80 (CCNc) in 2018. The combinations of the long-term particle number size distributions, total particle

81 number concentrations and CCN data at various Ss facilitate the utilisation of special methods for the data

82 validation and of joint evaluation procedures.

83

84 The major objective of the present study is to gain insight into the ~~droplet~~ cloud activation properties of

85 urban aerosol particles based on 1 measurement year in central Budapest. Specifically, we: ~~to~~ report,

86 discuss, explain and interpret here the measured time series and descriptive statistics of CCN

87 concentrations, ~~and~~the activated fractions of aerosol particles ~~for various Ss~~, ~~to determine~~ the effective

88 activation dry particle diameters, the ~~to compute~~ effective hygroscopicity parameters under various

89 supersaturated conditions and ~~to~~ formulate ~~derive~~ some common consequences of the data sets.

2 Methods

91 The time interval considered in this study was from 15 April 2019 to 14 April 2020. The number of days

92 with the CPC, DMPS, CCNc and meteorological measurements covered 100, 99, 85 and 100 % of the

93 relevant days, respectively. The CCNc was out of operation in January 2020. It is mentioned only for

94 completeness that t~~T~~he overall interval also involved the emergency phase (from 12 to 27 March 2020,

95 16 d) and the restriction on movement phase (from 28 March to the end of the measurement year, 18 d)

96 of the first outbreak of the COVID-19 pandemic in Hungary (Salma et al., 2020b). Local time

97 (LT=UTC+1 or daylight-saving time, UTC+2) was chosen as the time base of the data because it was

98 observed that the daily activity time pattern of inhabitants largely influences many atmospheric processes

99 in cities (Salma et al., 2014; Mikkonen et al., 2020).

2.1 Experimental part

101 All measurements were performed at the BpART Laboratory (N 47° 28' 30", E 19° 3' 45", 115 m above

102 mean sea level) of the Eötvös Loránd University (Salma et al., 2016). It represents an average atmospheric

103 environment for central Budapest due to its geographical location and meteorological conditions. Thus,

it can be regarded as an urban background site. The local sources comprise residential and household emissions including seasonal heating, exhaust of vehicle traffic and some industrial sources (Salma et al., 2017, 2020a, 2020b). Long-range transport of air masses can also play a role in shorter time intervals. The measurement site is located 85 m from the river Danube. The sampling inlets of the instruments were set up at heights between 12 and 13 m above the street level. Weather shield and insect net were only adopted to them. The laboratory was air conditioned at 20±3 ℃.

The CPC instrument deployed (TSI, model 3752, USA) was operated with an aerosol inlet flow of 1.5 L min^{-1}, and recorded concentrations of particles with a diameter above 4 nm using n-butanol as a working fluid. Its sampling inlet was made of stainless-steel tube with a diameter of 6.35 mm (¼ inch)(6.35 mm) and length of ca. 1.6 m. Mean particle number concentrations (N_{CPC}) with a time resolution of 1 min were extracted from its extended data base. The nominal specification of the CPC warrants an agreement in concentrations better than ±10 % between two identical instruments operating in the single-particle counting mode with a data averaging interval of >30 s.

The DMPS system utilised was a laboratory-made flow-switching-type device (University of Helsinki, Finland). It measured particle number concentrations in an electrical mobility diameter range from 6 to 1000 nm in the dry state of particles (with a relative humidity of RH<30 %) in 30 channels with a time resolution of 8 min (Salma et al., 2011, 2016). Its main components included a radioactive (^{60}Ni) bipolar diffusion charger, a monotube Nafion semi-permeable membrane dryer, a 28-cm-long Vienna-type differential mobility analyser and a butanol-based CPC (TSI, model 3775). The aerosol flow in the high and low modes were 2.0 and 0.31 L min^{-1}, respectively. The sheath flows were 10 times larger than the aerosol flows. The sampling inlet was made of copper tube with a diameter of 6 mm and length of ca. 1.9 m. The measurements were realised semi-continuously according to international technical standards (Wiedensohler et al., 2012; Schmale et al., 2017).

The CCNc system implemented was a DMT-200 instrument (Droplet Measurement Technologies, USA). It contains two vertical condensation chambers A and B of cylindrical shape (inner diameter 2.3 cm, length 50 cm; Roberts and Nenes, 2005; Rose et al., 2008). Their porous internal walls are continuously wetted with liquid water from peristaltic pumps. A linear positive temperature gradient along the cylinders is established and controlled at the top, middle and bottom zones of the chambers. The aerosol sample flow is continuously guided through the centre of the chambers and is surrounded by filtered sheath air flow. The flows proceed from top to bottom under laminar conditions and near-ambient air pressure (P). As the flows pass through the chambers, heat and water vapour are transported from the internal wall surface towards the centre of the chambers. Because water molecules diffuse faster than the air molecules (transferring the heat), a constant water vapour S is generated along the axes. Various Ss can be adjusted

by selecting different temperature gradients. The particles are exposed to this S for ca. 10 s. Those particles that activate at a critical S lower than the adjusted value form droplets. Their size is substantially larger than for inactivated particles. The droplets are detected at the exit of the chambers by optical particle counters as size distributions in a diameter range from 0.75 to 10 μm. The droplets larger than 1 μm are considered to be activated CCN, whereas the concentration of particles in this size interval is negligible.

The total air flow rates were set to 500 cm^3 min^{-1} and the ratio of the sample flow rate to the sheath flow rate was 1:10. The selected Ss were 0.1, 0.2, 0.3, 0.5 and 1.0 % stepping from the lowest to the highest values within a measuring cycle with duration times of 12, 5, 5, 5 and 5 min, respectively. The data measured by the system were recorded every 1 s. The CCN concentrations at a given S ($N_{\text{CCN},S}$) obtained by the two chambers should not differ by more than 15 %. The system was run in polydisperse operation mode largely according to the ACTRIS standard operation protocol (Gysel and Stratmann, 2013).

The meteorological measurements took place on site of the BpART Lab. Air temperature (T), RH, wind speed (WS), wind directions (WD), P and global solar radiation (GRad) were obtained by standardised meteorological sensors (HD52.3D17, Delta OHM, Italy and SMP3 pyranometer, Kipp and Zonen, the Netherlands) with a time resolution of 1 min as supporting information.

2.2 Data treatment and validation

The measured DMPS data were inverted into discrete size distributions, which were utilised to calculate particle number concentrations in the diameter ranges from 6 to 25 nm ($N_{6–25}$), from 6 to 100 nm ($N_{6–100}$), from 30 to 1000 nm ($N_{30–1000}$) and from 6 to 1000 nm ($N_{6–1000}$). The size intervals were selected to represent various important source types of particles and to maintain the comparison with earlier results. The extraction, treatment and processing of the measured CCNc data including the date and time, $N_{\text{CCN},S}$, flow rates and activation temperatures ($T_a=(T_1+T_2)/2$, with T_1 and T_2 as the read wall temperatures at the top and middle zones of the condensation chambers; Gysel and Stratmann, 2013) were accomplished for each S stage by a laboratory-developed computer software AeroSoLutions.

The averaging of the individual measured data was performed from the end of each S stage in a backward direction over a set time span within the temperature stability of the condensation chambers. The averaging times were determined by examining several randomly selected time-dependencies of CCN concentrations and temperatures in different seasons. The averaging intervals can be preselected for each S, and were ordinarily set to 90, 210, 210, 180 and 150 s, respectively for Ss of 0.1, 0.2, 0.3, 0.5 and 1.0 %. Their proper functioning was monitored within the data treatment, and they were refined for some individual cases if it was necessary. Warning flags on suspicious data were generated in the data processing, and the filtered data were checked separately. The two data sets for chambers A and B were

175 averaged if their ratio was <20 %. Otherwise, one of the two data sets was chosen on the basis of their

176 time evolution. For the S of 0.1 % (for small CCN concentrations), another averaging criterion, namely

177 ABS($N_{CCN,A}$–$N_{CCN,B}$)/min(SD$_{CCN,A}$, SD$_{CCN,B}$)<5 was utilised instead of the concentration ratio. The limits

178 were based upon exercises with concentrations in ordinary measurement intervals. They represent

179 sensible and pragmatic approaches, although alternative thresholds could also be set. Finally, it was

180 checked that the averaged CCN concentrations increased monotonically with S within the measurement

181 cycles. The time resolution of all experimental data derived from the CCNc instrument was 32 min.

182

183 The N_{6-1000} data from the DMPS system were compared to the CPC concentrations, which were averaged

184 over the corresponding DMPS measuring cycle. Due to the differences in the lowest measurable diameters

185 (6 vs. 4 nm, respectively), an agreement between the two instruments can be expected if the contribution

186 of nucleation-mode particles to total number of particles is negligible. Additional factor~~s~~ such as larger

187 particle transport losses along their longer path in the DMPS system and possibly different response times

188 of the two CPCs involved in the instruments could also contribute to the observed concentration

189 discrepancy~~add~~ (Salma et al., 2016). The comparison was realised by evaluating the N_{CPC}/N_{6-1000} ratio as

190 a function of the N_{6-30}/N_{6-1000} ratio. The intercept of their regression line was considered as the correction

191 factor for the DMPS system (Sect. 3.1).

192

193 For validation purposes, t~~T~~he CCN concentrations at the S of 1.0 % ($N_{CCN,1.0\%}$) were compared to the

194 particle number concentrations. ~~If most particles activate at this S then~~ T~~t~~he two concentrations are

195 expected to be similar if most particles activate at this S. In a previous survey, certain criteria were set to

196 exclude the time intervals when very small, hence, non-activating particles a~~we~~re present in larger

197 concentrations (Schmale at el., 2017). The comparison was performed under the conditions when the

198 concentration ratio of particles <30 nm to the total particles was <10 % or between 10 and 20 %. These

199 criteria were successfully adopted~~utilised~~ for remote or regional locations. However, T~~t~~he conditions

200 seem not to be applicable for urban data sets since their annual $N_{30-1000}/N_{6-1000}$ means and standard

201 deviations (SDs) ~~of the $N_{30-1000}/N_{6-1000}$ ratio~~are low with respect to more distant environments. In

202 Budapest, for instance, they were (52±15) %. This also caused that the relative number of the DMPS data

203 fulfilling either the criterium 1 or 2 above was~~ere~~ very small, i.e. only 2 % on a yearly scale. This is due

204 to relatively large and persistent contributions of high-temperature emission sources of particles typically

205 present in cities. The representativity of any conclusion for the whole data set derived on the basis of such

206 limited cases could to be statistically questioned.

207

208 To avoid this weak point, w~~W~~e propose here another criterium for urban or polluted environments as a

209 compromise between the larger relative number of cases and the constrained contribution of small, thus

210 non-activating particles. The $N_{CCN,1.0\%}$ data are only compared to the $N_{30-1000}$ data if the corresponding

ratio of $N_{30-1000}/N_{6-1000}$>70 %. This was fulfilled in a larger number of the DMPS concentrations and yielded more robust statistics, while the contribution of smaller particles remained still higher than for the original criteria. The limit value of 70% was determined in a pragmatic manner to express this compromise. Alternative values could also be set. The size distribution spectrum which date and time was the closest (within 20 min) and smaller than or equal to that of the CCN concentration was considered. The procedure is further discussed in Sect. 3.1.

2.3 ~~Modelling~~Particle hygroscopicity

For atmospheric aerosol, the activated fraction of particles tends to increase gradually with the dry particle diameter (as a sigmoid function instead of a step function valid for internally mixed monodisperse particles). This is primarily due to the fact that atmospheric particles are often external mixtures, or their chemical composition changes with particle size (Dusek et al., 2006; Rose et al., 2010). A threshold activation diameter, which is called effective critical dry particle diameter ($d_{c,eff}$) is defined in these cases as the size at which 50 % of the dry particles activate at a given S (Rose et al., 2008, 2010).

The effective critical dry particle diameters were assessed from collocated polydisperse CCN and particle number size distribution measurements as (Sihto et al., 2011; Kerminen et al., 2012; Schmale et al., 2018):

$$N_{\text{CCN},S} = \sum_{i=d_{c,eff}}^{d_{max}} N_i, \tag{1}$$

where d_{max} is the largest dry particle diameter measured by the sizing instrument (here DMPS) and N_i is the number of particles in the size channel i of the instrument. Hence, the concentrations were summed from the largest particle size (d_{max}) towards the smaller diameters until the measured CCN concentration was obtained. In order to estimate the $d_{c,eff}$ with higher accuracy, a logarithmic interpolation was accomplished between the last 2 diameters of the summation. The size distribution spectrum which date and time was the closest (with 20 min) and smaller than or equal to that of the CCN concentration was considered.

It has to be noted that the assumption of internally mixed particles is rarely met in urban environments including Budapest (Enroth et al., 2018). However, the approximation involves largely compensating influences, which still lead to reasonable results (Kammermann et al., 2020).

The cloud droplet activation of aerosol particles refers to their indefinite diameter growth (i.e. up to the droplet sizes) due to condensation of water vapour at constant saturation ratio ($s=p/p_0$ with p being the partial vapour pressure of water over a droplet solution and p_0 being the saturation vapour pressure of water over pure water with a flat surface). The conditions for the S_{eq} (with $S=s-1$) at which the droplets stay in equilibrium with the water vapour can be described by the Köhler model (e.g. Pruppacher and

Klett, 2000; McFiggans et al., 2006). To calculate the composition-dependent S_{eq} as function of the droplet diameter (d_{wet}) for a given dry particle diameter d_s, most controlling variables are further simplified and approximated within different types of thermodynamic parametrisations. In the present study, the effective hygroscopicity model was adopted (Petters and Kreidenweis, 2007). Laboratory and field measurements together with modelling considerations have indicated that this parametrisation proved to be a reliable under both sub- and supersaturation conditions (Rose et al., 2008; Merikanto et al., 2009; Rissler et al., 2010; Sihto et al., 2011; Kerminen et al., 2012; Schmale et al., 2018).

The S_{eq} can be expressed by assuming volume additivity of solute and water in the droplet and spherical shapes of the dry solute particle and solution droplet as (Petters and Kreidenweis, 2007):

$$S_{eq} = \frac{d_{wet}^3 - d_s^3}{d_{wet}^3 - d_s^3(1-\kappa)} \exp\left(\frac{A}{d_{wet}}\right) - 1, \qquad (2)$$

where

$$A = \frac{4\sigma_{d/a}M_w}{RT\rho_w}. \qquad (3)$$

The κ, $\underline{\sigma_{d/a},}$ M_w, ρ_w, R and T are the hygroscopicity parameter, surface tension of the droplet–air interface, molar mass of water (0.018015 kg mol^{-1}), density of water, the universal gas constant (8.3145 J mol^{-1} K^{-1}) and absolute temperature of the droplet and air in the thermodynamic equilibrium, respectively. The $\sigma_{d/a}$ was assumed to be that of pure water. Some organic chemical species in atmospheric aerosol particles such as humic-like substances are surface active and can lower the surface tension of the droplets (Facchini et al., 1999; Ovadnevaite et al., 2017). This depression is mainly controlled by diffusion of surfactants from the bulk of the droplet to its surface. It takes several hours to reach the thermodynamic equilibrium at medium concentrations (Salma et al., 2006). This implies that the possible alterations related to the lower surface tension than for the water are small with respect to estimated experimental uncertainties and can also be compensated by some surface/bulk partitioning effects (Sorjama et al., 2004). The surface tension of pure water seems, therefore, to be a reasonable approximation to reality under the conditions considered in the present study.

The κ values can be computed by solving Eq. 2. This contains several independent variables, i.e. T, d_s and d_{wet} in addition to the S_{eq} and κ value. The Ss are controlled by the CCNc instrument; the T can be expressed by the activation temperature in the condensation chamber (T_a, Sect. 2.2). For polydisperse atmospheric aerosol, d_s can be approximated by $d_{c,eff}$ (Eq. 1; Rose et al., 2008). An additional independent relationship, namely the fact that the dependency of S_{eq} on variable d_{wet} exhibits a maximum (of S_c at a diameter of d_c) is also exploited for solving Eq. 2. The κ values were computed in an iterative manner by

277 varying both κ and d_{wet} until the calculated Ss were equivalent to the adjusted Ss and at the same time, it

278 showed a maximum (Jurányi et al., 2010; Rose et al., 2010).

279

280 When the volume occupied by the solute can be neglected with respect to the water volume at the stage

281 of activation, the S_c can be approximated for κ>0.2 by (Petters and Kreidenweis, 2007):

282 $$\ln(S_c) = \sqrt{\frac{4A}{27} \frac{1}{\kappa d_c^3}}.$$ (4)

283

284 The time resolution of all modelled data was 32 min, which resulted in the total counts of data sets

285 typically 13.6×10^3 at each S level.

286 **3 Results and discussion**

287 The relevant meteorological properties for each month are summarised in Table S1 in the Supplement to

288 assist in creating the first impression on the actual atmospheric environment. They also indicate usual

289 weather conditions in Budapest during the measurement year without extraordinary situations.

290 **3.1 Data quality**

291 The DMPS measured systematically smaller total particle number concentrations (N_{6-1000}) than the CPC

292 (N_{CPC}) as discussed in Sect. 2.2. The intercept (a) and slope (b) with SDs of the regression line of the

293 N_{CPC}/N_{6-1000} ratio vs. N_{6-30}/N_{6-1000} ratio were a=1.33±0.01 and b=0.17±0.02, respectively and the

294 Pearsons's coefficient of correlation (R) between the concentration sets was 0.943. As a result of the

295 comparison, a size-independent multiplication correction factor of 1.33 was adopted for the inverted

296 DMPS data.

297

298 The scatter plot of the $N_{30-1000}$ DMPS data for which the $N_{30-1000}/N_{6-1000}$>70 % ($N_{30-1000,>70\%}$; see also Sect.

299 2.2) and the $N_{CCN,1.0\%}$ data is shown in Fig. 1a. It can be seen that all measured particle number

300 concentrations were larger than for the CCN. The $N_{30-1000,>70\%}/N_{CCN,1.0\%}$ ratio as function of $N_{CCN,1.0\%}$ (Fig.

301 1b) did not indicate systematic difference between the two instruments. Most concentration ratios with

302 larger (i.e. from ca. 3 to 7) values that showed up in all panels were isolated cases from each other. They

303 were most likely related to the time difference between the actual DMPS and CCNc data. Since the

304 instruments have time resolutions of ca. 8 min and 32 min, respectively, their compared data pairs could

305 have a time difference of up to 16 min (if the first possible DMPS measured spectrum was missing).

306 During this time span, the particle number concentrations could change substantially. Actual atmospheric

307 concentrations can vary rapidly because of the changes in intensity of some important anthropogenic

308 emission sources in the vicinity, of physical removal processes and in local meteorological conditions

309 (such as WS, which influences the particle transport). The dynamic ~~variability in concentrations often~~

310 ~~happens in~~is typical for cities and can be witnessed as suddenly appearing stripes on the particle number

311 size distribution surface plots (e.g. Fig. 10 in Salma et al., 2016).
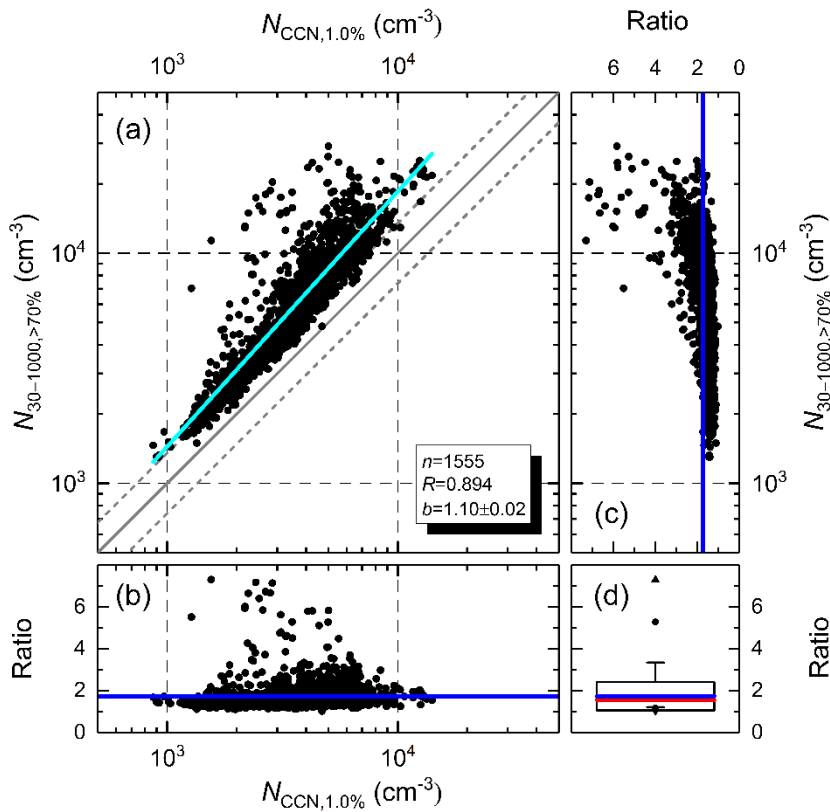
Figure 1. Relationship between the concentration of particles with a diameter >30 nm if their relative contribution to the total particles was >70 % ($N_{30-1000,>70\%}$) and CCN concentration at a supersaturation of 1.0 % ($N_{CCN,1.0\%}$; a). The number of the data points considered (n), their coefficient of correlation (R) and the slope (b) with SD of the regression line (in cyan) are also indicated. The line of equality and the dashed grey lines indicate the range of the expected uncertainty of ±15 % solely from particle counting. The $N_{30-1000,>70\%}/N_{CCN,1.0\%}$ ratios are also shown as function of the variables $N_{CCN,1.0\%}$ (b) and $N_{30-1000,>70\%}$ (c) with mean (the lines in blue colour). The box and whisker plot summarises the maximum and minimum (triangle pointing upward and downward, respectively), 1st and 99th percentiles (bullets), mean with SD (blue line and the horizontal borders of the box, respectively) and median (red line) of the $N_{30-1000,>70\%}/N_{CCN,1.0\%}$ ratios (d).

340 The $N_{30-1000,>70\%}/N_{CCN,1.0\%}$ ratio as function of $N_{30-1000,>70\%}$ (Fig. 1c) suggested that the ratio was slightly

341 increasing with the concentration, mainly above 10^4 cm^{-3}. An agreement between the $N_{30-1000,>70\%}$ and

342 $N_{CCN,1.0\%}$ is expected (approximately within ±15 %; Sect. 2.1) if the number of particles that were >30 nm

343 and that exhibited low hygroscopicity is negligible with respect to $N_{30-1000,>70\%}$. The opposite can be easily

344 realised in cities including Budapest. The argument is backed by the fact that the R between $N_{30-1000,>70\%}$

345 and N_{6-25} was significant (0.875) during the measurement year. The latter size fraction mainly contains

346 freshly emitted particles from road vehicles in most of the time (Salma et al., 2017), which typically

347 exhibit low hygroscopicity (Burkart et al., 2011; Rose et al., 2011; Enroth et al., 2018). They contribute

348 to the $N_{30-1000,>70\%}$ as well. Another indication of the chemical species with low hygroscopicity is the low

contribution of water-soluble organic carbon (WSOC) and high contribution of elemental carbon (soot) to organic carbon (OC), which are roughly related to general hygroscopicity, in central Budapest. The former ratio was substantially lower (WSOC/OC ratios from 20 to 39 %), while the latter ratio was considerably larger (EC/OC ratios from 14 to 20 %) in comparison with the aerosol that was already chemically aged or can be found above regional or remote areas (Salma et al., 2007, 2020a and references therein).

All this implies that the importance of the average $N_{30-1000,>70\%}/N_{CCN,1.0\%}$ ratio has to be extended or even preceded by the slope of the regression line and R of the two data sets as suggestive metrics for quality assurance. The mean ratio with SD and median ratio of $N_{30-1000,>70\%}/N_{CCN,1.0\%}$; the slope of the regression line with SD; and the coefficient of correlation for the overall data set were 1.73±0.67, 1.56, 1.10±0.02 and 0.894, respectively. Our set of quality indicators fits into the results of the data quality check elaborated for a number of other, mainly regional locations (Schmale et al., 2017). They jointly suggest that the CCNc and DMPS instruments were operating in a coherent manner and that the CCNc instrument performed reasonably well over the whole measurement year.

3.2 Concentrations and their ratios

The basic statistical measures of the particle number concentrations in different size fractions over the whole measurement year are summarised in Table 1. The mean ratio and SD of N_{6-100}/N_{6-1000} were (81±10) %. The concentrations are comparable with but somewhat larger than our earlier annual results, while the ratios agree well with the previous data (Mikkonen et al., 2020). The median particle number size distribution is shown in Fig. S1.

Table 1. Ranges, medians and means with SDs of the particle number concentrations in the diameter ranges from 6 to 25 nm (N_{6-25}), from 6 to 100 nm (N_{6-100}), from 30 to 1000 nm ($N_{30-1000}$), from 30 to 1000 nm if their contribution to total particles was >70 % ($N_{30-1000,>70\%}$) and from 6 to 1000 nm (N_{6-1000}) in a unit of 10^3 cm^{-3}.

Statistics	N_{6-25}	N_{6-100}	$N_{30-1000}$	$N_{30-1000,>70\%}$	N_{6-1000}
Min	0.069	0.66	0.26	0.81	0.76
Median	4.0	8.2	4.9	6.0	10.1
Max	137	153	47	39	154
Mean	5.3	10.1	6.0	7.2	12.1
SD	5.1	7.4	3.9	4.6	8.1

It is noted for completeness that the median N_{6-100} and N_{6-1000} during the restriction on movements of the first outbreak of the COVID-19 pandemic were smaller than the annual median levels by 72 and 79 %, respectively, while the $N_{30-1000}$ remained similar. The mean N_{6-100}/N_{6-1000} and SD of (75±12) % indicated

that the share of the ultrafine particles substantially decreased (cf. the previous paragraph). All this is in accordance with the conclusions of our more extensive study dedicated to this issue (Salma et al., 2020b).

The basic statistical measures of the CCN concentrations at different Ss over the whole measurement year are surveyed in Table 2. It is mentioned for completeness that some individual CCN concentrations at Ss of 0.5 and 1.0 % were above 9×10^3 cm^{-3} (Sect. 1), but only in 10 (0.073 % of all relevant data) and 59 cases (0.43 %), respectively, whereas the related κ values were rather low (Sect. 3.5). Therefore, the CCN-limited regime of droplet activation was realised. The median concentration changed monotonically from 0.59×10^3 to 2.5×10^3 cm^{-3} with S and showed a levelling off tendency. They were fitted by a power law function in the form of $N_{CCN,S}=c \times S^k$, where S is the supersaturation in % (in Origin Pro 2017 software using the Levenberg–Marquardt iteration algorithm) to obtain the so-called traditional CCN spectrum (Pruppacher and Klett, 2000). The constant c corresponds to the CCN concentration at an S of 1.0 %. The knowledge of these 2 parameters is sufficient for some cloud microphysics applications. The fitted parameters c and k with SDs obtained were $(2.81 \pm 0.12) \times 10^3$ cm^{-3} and 0.52 ± 0.05, respectively. The coefficient c agreed with the measured average $N_{CCN,1.0\%}$ (Table 2). The exponent k was within the interval reported for other continental locations (k=0.4–0.9; Pruppacher and Klett, 2000). The fitted function reproduced the experimental data at higher (>0.2 %) Ss satisfactorily, while their ratio became 1.25 at an S of 0.1 %. The comparison of the concentrations with other locations is accomplished together with the effective critical dry particle diameters in Sect. 3.3.

Table 2. Ranges, medians and means with SDs of the CCN concentrations (in $\times 10^3$ cm^{-3}) at supersaturations of 0.1, 0.2, 0.3, 0.5 and 1.0 %.

Statistics	0.1 %	0.2 %	0.3 %	0.5 %	1.0 %
Min	0.025	0.076	0.100	0.108	0.143
Median	0.59	1.09	1.39	1.80	2.5
Max	2.9	5.6	8.1	10.1	14.1
Mean	0.67	1.25	1.59	2.0	2.7
SD	0.41	0.74	0.97	1.2	1.5

The mean activation fractions (AF=$N_{CCN,S}/N_{6–1000}$) of the particles increased monotonically from 7 to 27 % with S and indicated some levelling off character (Fig. 2). The activation curve was obtained by fitting the experimental data with a two-parameter logarithm function of AF=$a \times \ln(S)+b$, where a and b are the fitting parameters (Paramonov et al., 2015) in Origin Pro 2017 software using the Levenberg–Marquardt iteration algorithm. Its shape was similar to that for the CCN concentrations. This is typical for non-coastal locations, where a multicomponent mixture of particle sources yield more-or-less balanced and, therefore, similar curves (Schmale et al., 2018). Figure 2 also contains the annual activation curve

obtained in a synthesis study of the European Aerosol Cloud Climate and Air Quality Interactions project by fitting the mean AFs for several regional and remote locations with an identical function (Fig. 5 in Paramonov et al., 2015). It can be seen that the curves for the urban and the other sites were rather different from each other in magnitudes or placement. The urban AFs were very substantially and systematically smaller than for the regional and remote locations. This was also witnessed with regard to other regional results (Sihto et al, 2011), and could be an urban feature. The low AF in cities can likely be explained by larger particle number concentrations, higher abundance of small particles that do not activate and by a chemical composition that can be characterised with typically lower hygroscopicity than for regional aerosol. At the same time, the relative SDs (RSDs) of our mean values were relatively high (between 45 and 70 %), which pointed to a considerable time variability of both N_{6-1000} and $N_{CCN,S}$. It also hinted that the prediction of CCN concentrations based solely on particle number concentrations and mean AFs are expected not to be reliable in urban environments. Moreover, the annual curves do not necessary capture the variability on shorter or seasonal scales.
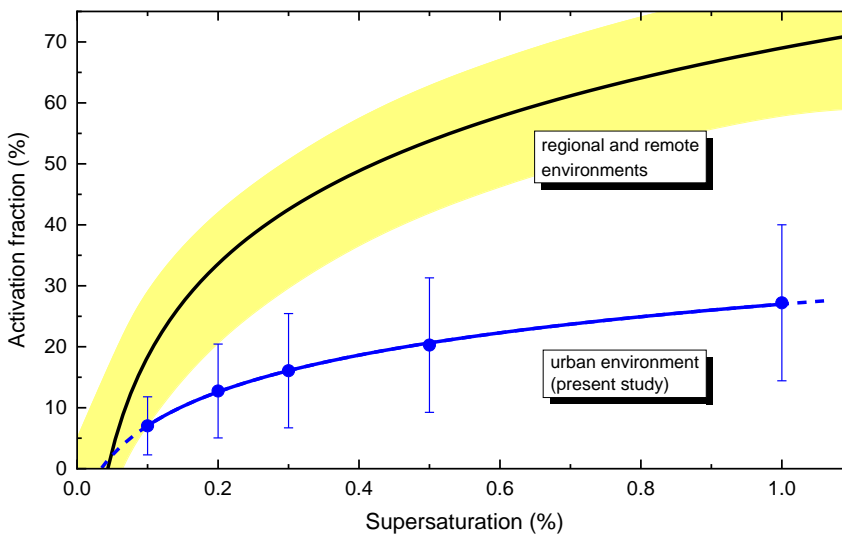
Figure 2. Mean activated fractions of total particles (N_{6-1000}) with SDs derived for central Budapest at supersaturations of 0.1, 0.2, 0.3, 0.5 and 1.0 % (experimental data in blue) together with their fitted dependency (line in blue). The fitting function was AF=$a\times$ln(S)+b, with parameters of a=34.8±0.4 and b=26.7±0.3. The line in black is shown for comparative purposes and was calculated by an identical function with the mean parameters of a=22 and b=69 that were obtained for several selected regional and remote sites in a EUCAARI synthesis study (Table 4; Paramonov et al., 2015). The yellow band represents the 95 % confidence interval. ~~The line serves to guide the eye.~~

3.3 Effective critical dry particle diameters

Basic statistical measures of the effective critical dry particle diameters at different Ss over the whole measurement year are displayed in Table 3. The median $d_{c,eff}$ decreased from 207 to 80 nm with S. All diameters were positioned within the accumulation mode of the median particle number size distribution (Fig. S1). The monthly mean number median mobility diameters for the Aitken and accumulation modes were typically 26 and 93 nm, respectively with an identical geometric SDs (GSDs) of 2.1 (Salma et al.,

2011). The broadening was caused by averaging the individual size distributions. Considering the minimum of the $d_{c,eff}$ data, some individual diameters, in particular for Ss of 0.5 and 1.0 %, could be shifted to the Aitken mode.

Table 3. Ranges, medians and means with SDs of the effective critical dry particle diameters in units of nm at supersaturations of 0.1, 0.2, 0.3, 0.5 and 1.0 %.

Statistics	0.1 %	0.2 %	0.3 %	0.5 %	1.0 %
Min	134	92	74	56	38
Median	207	149	126	105	80
Max	455	320	271	225	173
Mean	213	153	130	109	83
SD	32	26	24	22	20

The present average diameters and CCN concentrations were larger than for coastal or rural background, forested or remote environments (Henning et al., 2002; Komppula et al., 2005; Paramonov et al., 2015; Schmale et al., 2018). This confirmed that the water activation properties depend on the aerosol type. Our data were comparable with other urban sites (Kuwata and Kondo, 2008; Rose et al., 2010; Burkart et al., 2011; Meng et al., 2014). The modifications within the location category can likely be associated with relatively large differences between urban aerosol properties. The mean contributionshare and SD of ultrafine particles were, for instance, $N_{6-100}/N_{6-1000}=(81\pm10)$ % in Budapest and $N_{13-100}/N_{13-929}=75$ % in Vienna. The present $d_{c,eff}$ data were also contrasted with the computed results for the simulated global continental mean κ value and SD of 0.27 ± 0.21 (Pringle et al., 2010) in Fig. 3. The lines were obtained using the parameters given in Sect. 2.3. The data points belong to different parallel lines with a theoretical slope of $-3/2$. They suggested that the urban aerosol particles in Budapest with a diameter larger than approximately 130 nm showed similar hygroscopicity to continental aerosol in general, whereas the smaller particles appeared to be less hygroscopic. The distinctions were even larger when European continental aerosol is considered ($\kappa=0.36$; Pringle et al., 2010). The data points fairly tended toward the limiting relationship for insoluble but wettable particles by decreasing diameter. Freshly emitted soot particles could be an example of them (Rose et al., 2011).

The tendentious dependency of the deviation of the experimentally derived ($d_{c,eff}$, S_c) data points from the line for the simulated global continental mean κ (Fig. 3) also pointed to the size-dependent chemical composition, which is typicallikely more pronounced for urban particles. All this is in line with the ideas on the major source types such as vehicle emissions, biomass burning or new particle formation and diameter growth (NPF) events (Salma et al., 2014, 2017, 2020a, 2020b) and the particle number size distributions in Budapest (Salma et al., 2011). Photochemical processing may also play a role through

chemical ageing (Furutani et al., 2008). As a result, the urban sources often result in external mixtures of particles.
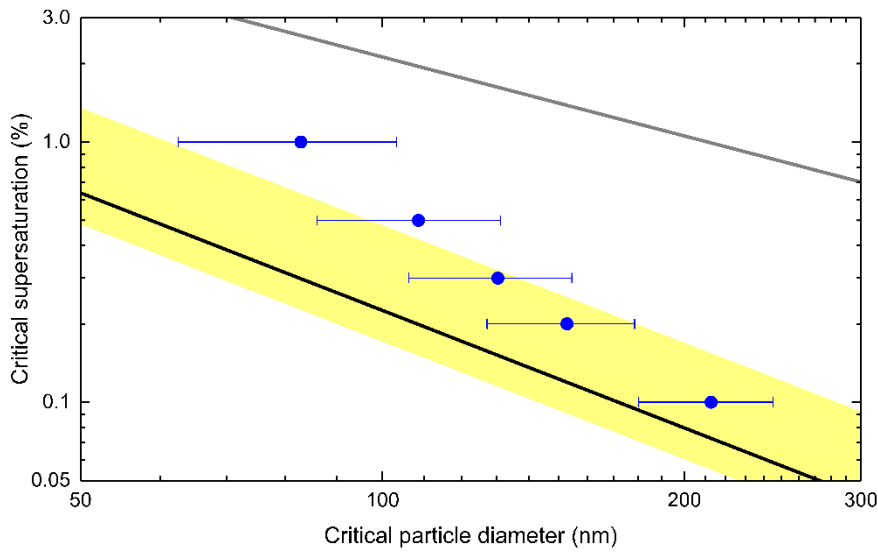
Figure 3. Critical supersaturation and effective critical dry particle diameter data pairs with SDs (in blue) determined experimentally in central Budapest and the dependency calculated for the simulated global continental mean κ and SD of 0.27±0.21. The line in black was obtained for the mean κ value and the yellow band represents ±1 SD. The relationship for insoluble but wettable particles (κ=0, the Kelvin term) was displayed by the line in grey for comparative purposes.

Frequency distributions of $d_{c,eff}$ at an S can be described by a lognormal distribution function. The normalised differential distributions of the $d_{c,eff}$ data for each S are shown in Fig. 4. They were derived by partitioning all diameter data into 71 intervals with an equal width of 0.0243 on logarithmic scale between 10 and 500 nm. The selections proved to be a reasonable compromise between the good statistics and good data resolution. The distributions exhibited single peaks with geometric SDs increasing monotonically with S as 1.14, 1.16, 1.20, 1.22 and 1.27, respectively. The broadening indicated larger variability in droplet activation properties of the smaller particles.

The peaks exhibited a fine structure. They seemed to contain submodes. This is likely related to the mixtures of particles with different activation properties. The submodes could be produced by sources which result in particles with different chemical composition and mixing states. These differences may not necessarily show up in the particle number size distributions, while they can lead to diverse activation properties. Several compositional elements of the fine structure (e.g. the maximum or the relative peak areas) changed in a tendentious manner by S. Their exact identification and interpretation are beyond the objectives of the present paper. They are to be included into an upcoming study which is to deal with the relationships of major source types such as vehicle emissions, NPF events or biomass burning and the activation properties of CCN together with their diurnal variability and air mass trajectories.
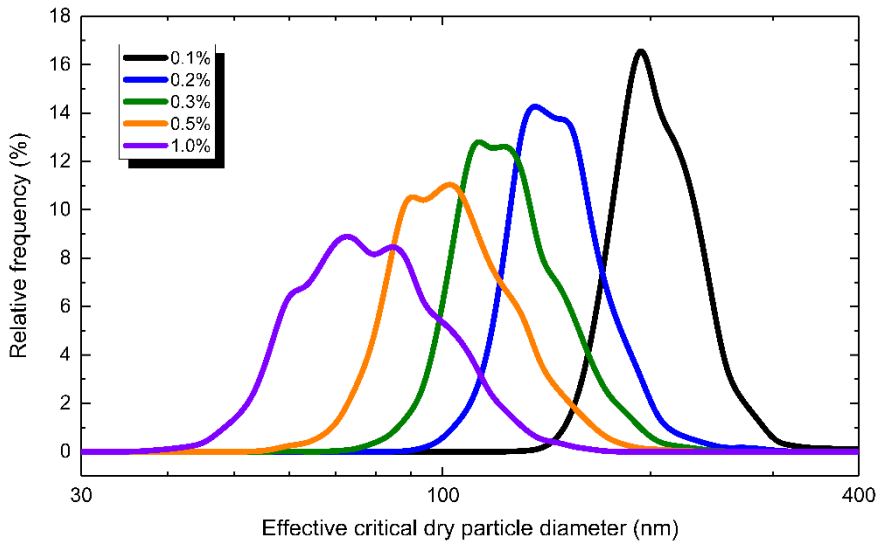
Figure 4. Differential frequency distributions of effective critical dry particle diameters at supersaturations of 0.1, 0.2, 0.3, 0.5 and 1.0 % normalised to the total counts of the diameter data.

3.4 Seasonal cycling

The time series of the experimental data showed high variability in time. The monthly medians seemed to be more advantageous for investigating the possible seasonal cycling (Fig. 5). It is noted that medians were selected as characteristics instead of means and SDs since these probability variables can be described by lognormal distribution functions (Sect. 3.2). The months were organised to represent the spring (MAM), summer (JJA), autumn (SON) and winter (DJF) seasons. The Stricter chronological ordering of the months seems to be more advantageous for source-related or dynamic studies on various timescales.

The dependencies for the separate variables were similar to each other at different Ss. The changes were pronounced mainly for the larger Ss, which are the least relevant for an ambient air. This already indicates that the seasonal cycling does not very likely or substantially influence the aerosol–water vapour interactions under ordinary environmental conditions. The CCN concentrations appeared somewhat smaller from May to September, and somewhat larger in the other months. Their minimum was typically in May. These intervals coincided with the non-heating (formally from 15 April to 15 October) and heating seasons (the rest of the year) in Hungary. As an exception, the concentrations for February were unusually small. The AFs appeared to be smaller in May (and perhaps also in June) and September (and perhaps also in October), and larger in the other months. The comparison of the monthly median $N_{CCN,S}$ and AF to the dependency of the total particle numbers implied that the seasonal variations of the former two properties were not mainly due to the variations in the particle number concentrations. No obvious dependency for the monthly median $d_{c,eff}$ values could be established since their distributions were featureless. The lack of cycling meant that the particles in Budapest exhibited more or less similar droplet activation behaviour over the year. This was different from some other, non-urban locations (Pringle et

al., 2010; Sihto et al., 2011; Paramonov et al., 2013, 2015; Schmale et al., 2018). It is also noted that the *d*c,eff values for an *S* of 0.1 % ~~*S*~~ were segregated somewhat ~~segregated~~ more from the other dependencies. It has to be added that March and ~~May~~ April 2020 were extraordinary due to the first outbreak of the COVID-19 pandemic in Hungary. Firmer seasonal dependencies require longer measurements since the related properties can also be influenced by inter-annual variability.
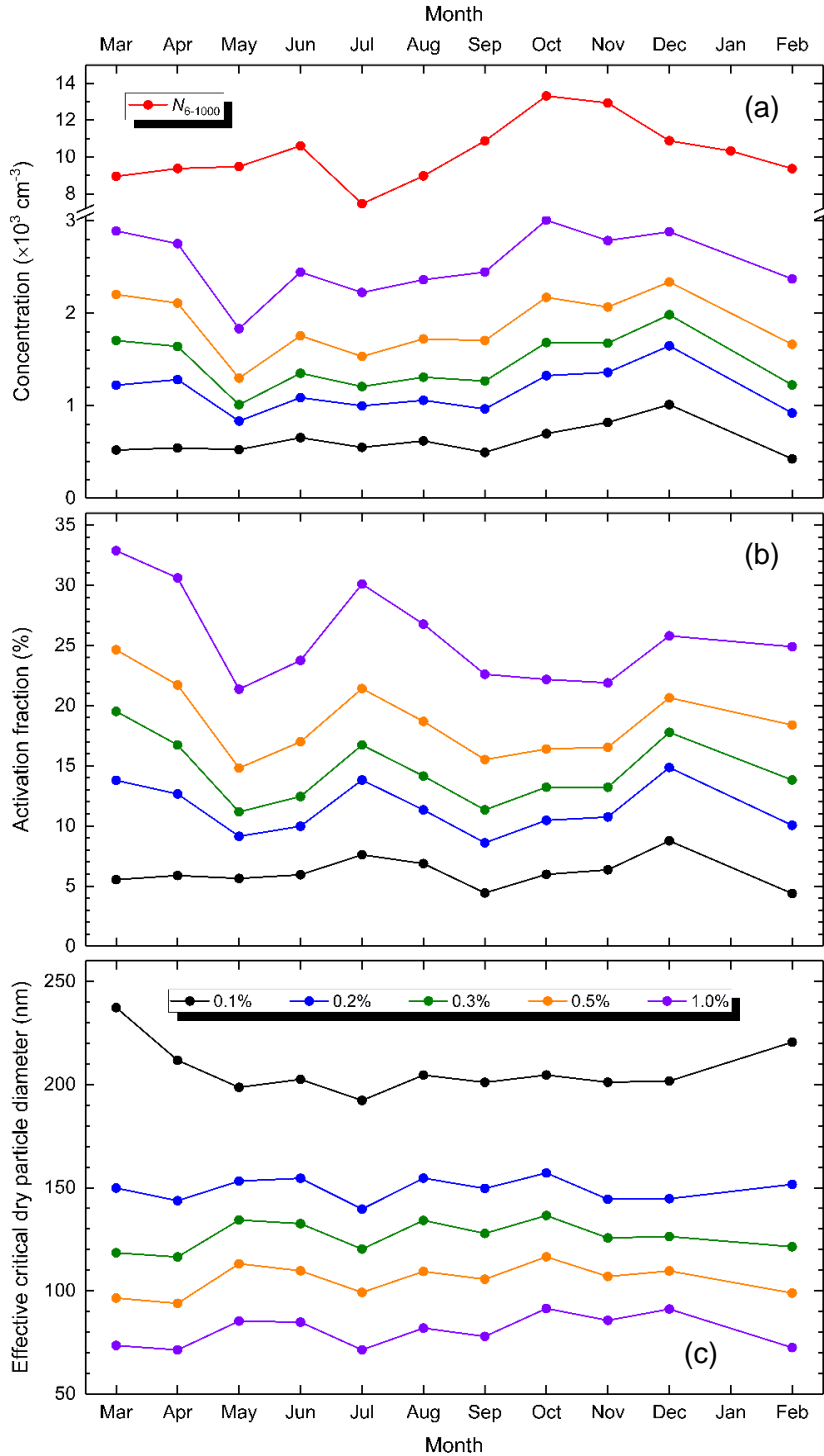
Figure 5. Time series of the monthly median CCN concentrations and total particle number concentration (N_{6-1000}; a), activation fractions (b) and effective critical dry particle diameters (c) at supersaturations of 0.1, 0.2, 0.3, 0.5 and 1.0 %.

~~Taking into account that Ss~~Supersaturations of ~~only~~ ca. 0.1 % ordinarily occur in warm stratiform clouds, and ~~that~~ these Ss ~~ordinarily~~ activate only larger ($d>200$ nm) particles. ~~, it can be concluded that the~~ ~~e~~Chemical composition of these ~~larger~~ particles ~~were~~ are usually more balanced over the year than for smaller particles due to, for instance, chemical and physical ageing and particle mixing processes. Therefore, ~~I~~it ~~, therefore,~~ can be concluded that differences in chemical composition ~~do~~es not seem to play a crucial role in cloud ~~CCN~~ activation properties even in cities. ~~It has to be added that March and May April 2020 were extraordinary due to the first outbreak of the COVID-19 pandemic in HungaryFirmer seasonal dependencies require longer continuous measurements since the related properties can be also influenced by inter annual differences in chemical composition, aerosol and meteorological properties and in biogenic cycling~~.

3.5 Hygroscopicity parameters

The basic statistical measures of the κ values for different Ss over the whole measurement year are given in Table 4. All characteristics decreased monotonically and showed a levelling off tendency with S. The averages implied in general that the larger particles exhibited higher hygroscopicity than the smaller particles. When considering also the $d_{c,eff}$ data which belong to the Ss, the present hygroscopicity parameters fairly agreed with the values derived previously from volatility and hygroscopicity tandem differential mobility analyser (VH-TDMA) measurements under subsaturated conditions (RH=90 %) at the identical site (Enroth et al., 2018). In that study, the nearly hydrophobic particles exhibited a mean κ value of 0.033. The mode typically contained 69 % of particles at a dry diameter of 50 nm, and the κ seemed to be independent of the particle diameter in the range from 50 to 145 nm. The less hygroscopic particles showed larger mean κ value of 0.20. They typically made up 59 % of particles at 145 nm.

Table 4. Ranges, medians and means with SDs for the hygroscopicity parameter at supersaturations of 0.1, 0.2, 0.3, 0.5 and 1.0 %.

Statistics	0.1 %	0.2 %	0.3 %	0.5 %	1.0 %
Min	0.014	0.010	0.006	0.003	0.0003
Median	0.149	0.099	0.071	0.043	0.021
Max	0.47	0.42	0.35	0.29	0.22
Mean	0.154	0.106	0.078	0.049	0.027
SD	0.061	0.048	0.041	0.031	0.022

The average κ values were considerably smaller than for regional or remote locations (Paramonov et al., 2015; Schmale et al., 2018). There are few hygroscopicity parameters reported specifically for urban environments, and even less for city centres (Gunthe et al., 2011; Rose et al., 2010, 2011; Meng et al., 2014; Arub et al., 2020). The present data can also be linked to the average or effective hygroscopicity

parameters found in field measurements and chamber studies for fresh soot particles of <0.01, for secondary organic aerosol of approximately 0.10 and for inorganic aerosol fraction of ca. 0.64 (Rose et al., 2011). All this pointed to the presence of freshly emitted and externally mixed soot particles with very low hygroscopicity in high abundancies in central Budapest.
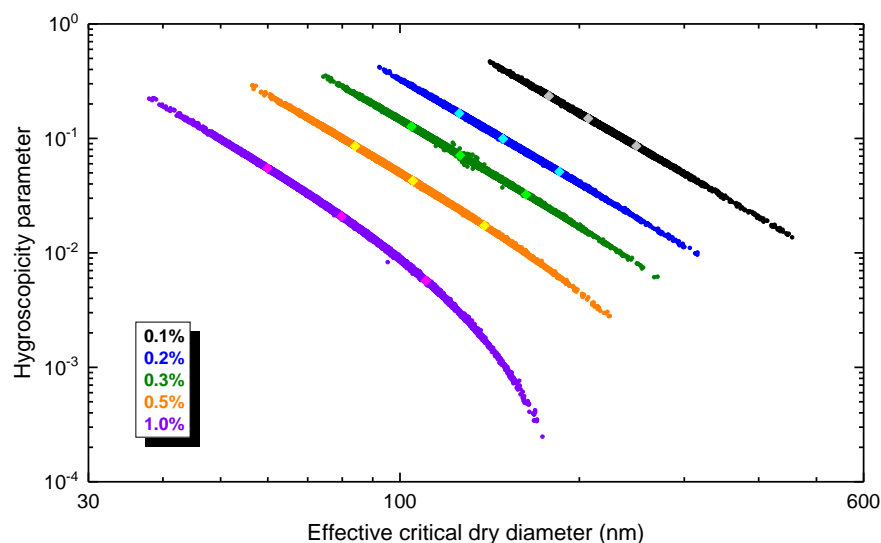
Figure 6. Relationship of the hygroscopicity parameter and the effective critical dry particle diameter ($d_{c,eff}$) derived at supersaturations of 0.1, 0.2, 0.3, 0.5 and 1.0 %. The three diamond symbols in lighter colours on each data set represent the data pairs belonging to the 10th and 90th percentiles; 50th and 50th percentiles; and 90th and 10th percentiles in the order of increasing $d_{c,eff}$.

The range of the κ values was increasing with *S*, and, more importantly, it became particularly large (a factor of ca. 10^3 for 1.0 %) even when compared with aerosol properties typically driven by atmospheric dynamics. This can be illustrated by the relationships between the κ value and $d_{c,eff}$ for each *S* (Fig. 6). The data sets created separate lines or narrow stripes with a theoretical slope of –3 over the main range of the variables considered assuming that the other physicochemical properties such as d_{wet}, T_a, $\sigma_{d/a}$ and ρ_w do not change substantially. The line for the *S* of 1.0 % was bended at low κ and large $d_{c,eff}$. This is also in accordance with the κ–Köhler model (Eq. 2). It can be seen that the data pairs shown for a given *S* level indeed cover a wide interval of the related variables. Such variability in κ did not back the idea of using just a single characteristic value for a given *S*, and an effective κ parameter or its function on particle size would be preferred instead (Paramonov et al., 2015). The average hygroscopicity parameter represented the particles with a size close to the effective critical dry particle diameter. Furthermore, the distributions of the data pairs along the lines were not completely symmetric with respect to the medians, which confirmed the fine structure of the frequency distributions (Sect. 3.3). The 3 characteristic points (10th, 50th and 90th percentiles) on the lines indicated a broadening of the frequency distributions with *S*. The frequency distribution of the hygroscopicity parameters in 71 intervals with an equal width of 0.0571

662 on logarithmic scale between 10^{-4} and 10^{0} are shown in Fig. S2. They largely reflect the behaviour and

663 tendencies of the effective critical dry particle diameter (Fig. 4) since their computations involved $d_{c,eff}$.

4 Conclusions

665 Concentrations of CCN at various Ss and particle number size distributions were measured in parallel

666 with each other in a continental central European urban environment over 1 year. The effective cloud

667 droplet activation properties of the aerosol population were determined from the available experimental

668 data without measuring the time-resolved chemical composition. The results indicated several urban

669 specialities. The average CCN concentrations were substantially larger, whereas the average effective

670 critical dry particle diameters and activation fractions were considerably and systematically smaller than

671 for non-urban sites. The particles with a diameter of ca. <130 nm already showed lower hygroscopicity

672 than in general, and the difference between the urban and general hygroscopic properties ~~it~~ was further

673 enhanced ~~decreasing even more with~~ for ~~lower~~ decreasing size. These urban features can likely be related

674 to the high abundance of freshly emitted less-hygroscopic particles including soot and to substantial

675 differences in the size-dependent chemical composition and mixing states of particles in cities. The

676 seasonal dependencies ~~of the~~in N_{CCN} and activation fractions at various Ss ~~derived properties~~were only

677 loosely connected to ~~not pronounced or obvious and could not be explained solely by variations in~~ the

678 total particle number concentrations. The achieved results represent the first information of this type for

679 a city in the Carpathian Basin and contribute to our general knowledge on and understanding of urban

680 atmospheric environments.

681

682 The measurements were performed at a fix location in central Budapest, which can be regarded as an

683 urban background site. The obtained results and conclusions are representative for the average or overall

684 atmosphere of the city centre. Some urban microenvironments such as kerbside sites, street canyons, road

685 junctions or suburban areas exhibit diverse size distributions and chemical composition, and, therefore,

686 certain differences in hygroscopic properties are expected among them. Furthermore, some relevant

687 meteorological conditions can also change within the urban canopy due to, for instance, heat islands often

688 realised in large cities. At the same time, the related atmospheric processes likely occur on larger spatial

689 scales than the city itself or its central part. From this point of view, the data derived for the urban

690 background appear to be a sensible starting approximation to reality. Further dedicated studies preferably

691 involving surface measurements, satellite products and modelling can contribute to an understanding of

692 the challenging issue of the urban climate.

693

694 The water uptake properties of urban aerosol particles under both sub- and supersaturation conditions are

695 increasingly recognised also because of their relevance in urban climate considerations and in particle

deposition modelling in the human respiratory system. The κ values determined here are to be further utilised in health-related studies as well.

After gaining experience with operation and calibration of the dual-chamber CCNc measurement system, we plan to extend one of its chambers by a DMA and CPC setup so we can perform both polydisperse and monodisperse measurements in parallel, which is expected to supply further valuable knowledge on the mixing states of particles. This is especially important since urban aerosol particles typically comprise externally mixed carbonaceous particles with very distinct hygroscopic properties. This seems to be relevant in general and could also support or facilitate the association of the hygroscopicity parameters to major source types in cities together with multistatistical apportionment methods.

Data availability. The observational data are available from the corresponding author.

Supplement. The supplement related to this article is available online:

Author contributions. IS conceived, designed and lead the research; WT and AZGy performed the measurements; MV developed the ASL data evaluation software; IS, MV and WT accomplished the data treatment and prepared the figures; IS, WT, MV and AZGy interpreted the results; IS wrote the manuscript with comments from all coauthors.

Competing interests. The authors declare that they have no conflict of interest.

Financial support. This research has been supported by the Hungarian Research, Development and Innovation Office (grant no. K132254) and by the European Regional Development Fund and the Hungarian Government (GINOP-2.3.2-15-2016-00028).

References

Andreae, M. O. and Rosenfeld, D.: Aerosol-cloud-precipitation interactions. Part 1. The nature and sources of cloud-active aerosols, Earth Sci. Rev., 89, 13–41, https://doi.org/10.1016/j.earscirev.2008.03.001, 2008.

Andreae, M. O., Jones, C. D., and Cox, P. M.: Strong present-day aerosol cooling implies a hot future, Nature, 435, 1187–1190, https://doi.org/10.1038/nature03671, 2005.

Arub, Z., Bhandari, S., Gani, S., Apte, J. S., Hildebrandt Ruiz, L., and Habib, G.: Air mass physiochemical characteristics over New Delhi: impacts on aerosol hygroscopicity and cloud condensation nuclei (CCN) formation, Atmos. Chem. Phys., 20, 6953–6971, https://doi.org/10.5194/acp-20-6953-2020, 2020

Burkart, J., Steiner, G., Reischl, G., and Hitzenberger, R.: Longterm study of cloud condensation nuclei (CCN) activation of the atmospheric aerosol in Vienna, Atmos. Environ., 45, 5751–5759, https://doi.org/10.1016/j.atmosenv.2011.07.022, 2011.

Carslaw, K., Lee, L., Reddington, C., Pringle, K., Rap, A., Forster, P., Mann, G., Spracklen, D., Woodhouse, M., and Regayre, L.: Large contribution of natural aerosols to uncertainty in indirect forcing, Nature, 503, 67–71, https://doi.org/10.1038/nature12674, 2013.

Dusek, U., Frank, G. P., Hildebrandt, L, Curtius, J., Schneider, J., Walter, S., Chand, D., Drewnick, F., Hings, S., Jung, D., Bormann, S., and Andreae, M. O.: Size matters more than chemistry for cloud-nucleating ability of aerosol particles, Science, 312, 1375–1378, https://doi.org/10.1126/science.1125261, 2006.

Enroth, J., Mikkilä, J., Németh, Z., Kulmala, M., and Salma, I.: Wintertime hygroscopicity and volatility of ambient urban aerosol particles, Atmos. Chem. Phys., 18, 4533–4548, https://doi.org/10.5194/acp-18-4533-2018, 2018.

Facchini, M. C., Mircea, M., Fuzzi, S., and Charlson, R. J.: Cloud albedo enhancement by surface-active organic solutes in growing droplets, Nature, 401, 257–259, https://doi.org/10.1038/45758, 1999.

Furutani, H., Dall'osto, M., Roberts, G. C., and Prather, K. A.: Assessment of the relative importance of atmospheric aging on CCN activity derived from measurements, Atmos. Environ., 42, 3130–3142, https://doi.org/10.1016/j.atmosenv.2007.09.024, 2008.

Gunthe, S. S., Rose, D., Su, H., Garland, R. M., Achtert, P., Nowak, A., Wiedensohler, A., Kuwata, M., Takegawa, N., Kondo, Y., Hu, M., Shao, M., Zhu, T., Andreae, M. O., and Pöschl, U.: Cloud condensation nuclei (CCN) from fresh and aged air pollution in the megacity region of Beijing, Atmos. Chem. Phys., 11, 11023–11039, https://doi.org/10.5194/acp-11-11023-2011, 2011.

Gysel, M. and Stratmann, F.: WP3 – NA3: In-situ chemical, physical and optical properties of aerosols, Deliverable D3.11: Standardized protocol for CCN measurements, Tech. rep., available at: https://studylib.net/doc/18744398/standardized-protocol-for-long-term-cloud-condensation (last access: 2 April 2021), 2013.

Henning, S., Weingartner, E., Schmidt, S., We11ndisch, M., Gäggeler, H. W., and Baltensperger, U.: Size-dependent aerosol activation at the high-alpine site Jungfraujoch (3580m a.s.l.), Tellus B, 54, 82–95, https://doi.org/10.3402/tellusb.v54i1.16650, 2002.

Herenz, P., Wex, H., Henning, S., Kristensen, T. B., Rubach, F., Roth, A., Borrmann, S., Bozem, H., Schulz, H., and Stratmann, F.: Measurements of aerosol and CCN properties in the Mackenzie River delta (Canadian Arctic) during spring–summer transition in May 2014, Atmos. Chem. Phys., 18, 4477–4496, https://doi.org/10.5194/acp-18-4477-2018, 2018.

Hudson, J.: Variability of the relationship between particle size and cloud nucleating ability, Geophys. Res. Let., 34, L08801, https://doi.org/10.1029/2006GL028850, 2007.

Jurányi, Z., Gysel, M., Weingartner, E., DeCarlo, P. F., Kammermann, L., and Baltensperger, U.: Measured and modelled cloud condensation nuclei number concentration at the high alpine site Jungfraujoch, Atmos. Chem. Phys., 10, 7891–7906, https://doi.org/10.5194/acp-10-7891-2010, 2010.

Jurányi, Z., Gysel, M., Weingartner, E., Bukowiecki, N., Kammermann, L., and Baltensperger, U.: A 17 month climatology of the cloud condensation nuclei number concentration at the high alpine site Jungfraujoch, J. Geophys. Res.-Atmos., 116, D10204, https://doi.org/10.1029/2010JD015199, 2011.

Kammermann, L., Gysel, M., Weingartner, E., Herich, H., Cziczo, D. J., Holst, T., Svenningsson, B., Arneth, A., and Baltensperger, U.: Subarctic atmospheric aerosol composition: 3. Measured and modeled properties of cloud condensation nuclei, J. Geophys. Res., 115, 04202, https://doi.org/10.1029/2009JD012447, 2010.

Kerminen, V.-M., Paramonov, M., Anttila, T., Riipinen, I., Fountoukis, C., Korhonen, H., Asmi, E., Laakso, L., Lihavainen, H., Swietlicki, E., Svenningsson, B., Asmi, A., Pandis, S. N., Kulmala, M., and Petäjä, T.: Cloud condensation nuclei production associated with atmospheric nucleation: a synthesis based on existing literature and new results, Atmos. Chem. Phys., 12, 12037–12059, https://doi.org/10.5194/acp-12-12037-2012, 2012.

Komppula, M., Lihavainen, H., Kerminen, V.-M., Kulmala, M., and Viisanen, Y.: Measurements of cloud droplet activation of aerosol particle at a clean subarctic background site, J. Geophys. Res., 110, 06204, https://doi.org/10.1029/2004JD005200, 2005.

Kuwata, M. and Kondo Y.: Dependence of size-resolved CCN spectra on the mixing state of nonvolatile cores observed in Tokyo, J. Geophys. Res., 113, 19202, https://doi.org/10.1029/2007JD009761, 2008.

McFiggans, G., Artaxo, P., Baltensperger, U., Coe, H., Facchini, M.-C., Feingold, G., Fuzzi, S., Gysel, M., Laaksonen, A., Lohmann, U., Mentel, T. F., Murphy, D. M., O'Dowd, C. D., Snider, J. R., and Weingartner, E.: The effect of physical and chemical aerosol properties on warm cloud droplet activation, Atmos. Chem. Phys., 6, 2593–2649, https://doi.org/10.5194/acp-6-2593-2006, 2006.

Merikanto, J., Spracklen, D. V., Mann, G. W., Pickering, S. J., and Carslaw, K. S.: Impact of nucleation on global CCN, Atmos. Chem. Phys., 9, 8601–8616, https://doi.org/10.5194/acp-9-8601-2009, 2009.

Mikkonen, S., Németh, Z., Varga, V., Weidinger, T., Leinonen, V., Yli-Juuti, T., and Salma, I.: Decennial time trends and diurnal patterns of particle number concentrations in a central European city between 2008 and 2018, Atmos. Chem. Phys., 20, 12247–12263, https://doi.org/10.5194/acp-20-12247-2020, 2020.

Meng, J. W., Yeung, M. C., Li, Y. J., Lee, B. Y. L., and Chan, C. K.: Size-resolved cloud condensation nuclei (CCN) activity and closure analysis at the HKUST Supersite in Hong Kong, Atmos. Chem. Phys., 14, 10267–10282, https://doi.org/10.5194/acp-14-10267-2014, 2014.

Ovadnevaite, J., Zuend, A., Laaksonen, A., Sanchez, K. J., Roberts, G., Ceburnis, D., Decesari, S., Rinaldi, M., Hodas, N., Facchini, M. C., Seinfeld, J. H., and O'Dowd, C.: Surface tension prevails over solute effect in organic-influenced cloud droplet activation, Nature, 546, 637–641, https://doi.org/10.1038/nature22806, 2017.

Paramonov, M., Aalto, P. P., Asmi, A., Prisle, N., Kerminen, V.-M., Kulmala, M., and Petäjä, T.: The analysis of size-segregated cloud condensation nuclei counter (CCNC) data and its implications for cloud droplet activation, Atmos. Chem. Phys., 13, 10285–10301, https://doi.org/10.5194/acp-13-10285-2013, 2013.

Paramonov, M., Kerminen, V.-M., Gysel, M., Aalto, P. P., Andreae, M. O., Asmi, E., Baltensperger, U., Bougiatioti, A., Brus, D., Frank, G. P., Good, N., Gunthe, S. S., Hao, L., Irwin, M., Jaatinen, A., Jurányi, Z., King, S. M., Kortelainen, A., Kristensson, A., Lihavainen, H., Kulmala, M., Lohmann, U., Martin, S. T., McFiggans, G., Mihalopoulos, N., Nenes, A., O'Dowd, C. D., Ovadnevaite, J., Petäjä, T., Pöschl, U., Roberts, G. C., Rose, D., Svenningsson, B., Swietlicki, E., Weingartner, E., Whitehead, J., Wiedensohler, A., Wittbom, C., and Sierau, B.: A synthesis of cloud condensation nuclei counter (CCNC) measurements within the EUCAARI network, Atmos. Chem. Phys., 15, 12211–12229, https://doi.org/10.5194/acp-15-12211-2015, 2015.

Petters, M. D. and Kreidenweis, S. M.: A single parameter representation of hygroscopic growth and cloud condensation nucleus activity, Atmos. Chem. Phys., 7, 1961–1971, https://doi.org/10.5194/acp-7-1961-2007, 2007.

Pringle, K. J., Tost, H., Pozzer, A., Pöschl, U., and Lelieveld, J.: Global distribution of the effective aerosol hygroscopicity parameter for CCN activation, Atmos. Chem. Phys., 10, 5241–5255, https://doi.org/10.1007/978-0-306-48100-010.5194/acp-10-5241-2010, 2010.

Pruppacher, H. R. and Klett, J. D.: Microphysics of clouds and precipitation, Kluwer, Dordrecht, https://doi.org/10.1007/978-0-306-48100-0, 2000.

Rissler, J., Svenningsson, B., Fors, E. O., Bilde, M., and Swietlicki, E.: An evaluation and comparison of cloud condensation nucleus activity models: Predicting particle critical saturation from growth at subsaturation, J. Geophys. Res., 115, 22208, https://doi.org/10.1029/2010JD014391, 2010.

Roberts, G. and Nenes, A.: A continuous-flow streamwise thermal-gradient CCN chamber for atmospheric measurements, Aerosol Sci. Tech., 39, 206–221, https://doi.org/10.1080/027868290913988, 2005.

Rose, D., Gunthe, S. S., Mikhailov, E., Frank, G. P., Dusek, U., Andreae, M. O., and Pöschl, U.: Calibration and measurement uncertainties of a continuous-flow cloud condensation nuclei counter (DMT-CCNC): CCN activation of ammonium sulfate and sodium chloride aerosol particles in theory and experiment, Atmos. Chem. Phys., 8, 1153–1179, https://doi.org/10.5194/acp-8-1153-2008, 2008.

Rose, D., Nowak, A., Achtert, P., Wiedensohler, A., Hu, M., Shao, M., Zhang, Y., Andreae, M. O., and Pöschl, U.: Cloud condensation nuclei in polluted air and biomass burning smoke near the mega-city Guangzhou, China – Part 1: Size-resolved measurements and implications for the modeling of aerosol particle hygroscopicity and CCN activity, Atmos. Chem. Phys., 10, 3365–3383, https://doi.org/10.5194/acp-10-3365-2010, 2010.

Rose, D., Gunthe, S. S., Su, H., Garland, R. M., Yang, H., Berghof, M., Cheng, Y. F., Wehner, B., Achtert, P., Nowak, A., Wiedensohler, A., Takegawa, N., Kondo, Y., Hu, M., Zhang, Y., Andreae, M. O., and Pöschl, U.: Cloud condensation nuclei in polluted air and biomass burning smoke near the mega-city Guangzhou, China – Part 2: Size-resolved aerosol chemical composition, diurnal cycles, and externally mixed weakly CCN-active soot particles, Atmos. Chem. Phys., 11, 2817–2836, https://doi.org/10.5194/acp-11-2817-2011, 2011.

Rosenfeld, D., Lohmann, U., Raga, G. B., O'Dowd, C. D., Kulmala, M., Fuzzi, S., Reissell, A., and Andreae, M. O.: Flood or drought: How do aerosols affect precipitations?, Science, 321, https://doi.org/1309–1313, 10.1126/science.1160606, 2008.

Rosenfeld, D., Andreae, M. O., Asmi, A., Chin, M., de Leeuw, G., Donovan, D. P., Kahn, R., Kinne, S., Kivekäs, N., Kulmala, M., Lau, W. Sebastian Schmidt, K., Suni, T., Wagner, T., and Wild, M.: Global observations of aerosol-cloud-precipitation-climate interactions, Rev. Geophys., 52, 750–808, https://doi.org/10. 1002/2013RG000441, 2014.

Salma, I., Ocskay, R., Varga, I., and Maenhaut, W.: Surface tension of atmospheric humic-like substances in connection with relaxation, dilution, and solution pH, J. Geophys. Res., 111, D23205, https://doi.org/10.1029/2005JD007015, 2006.

Salma, I., Ocskay, R., Chi, X., and Maenhaut, W.: Sampling artefacts, concentration and chemical composition of fine water-soluble organic carbon and humic-like substances in a continental urban atmospheric environment, Atmos. Environ., 41, 4106–4118, https://doi.org/10.1016/j.atmosenv.2007.01.027, 2007.

Salma, I., Borsós, T., Weidinger, T., Aalto, P., Hussein, T., Dal Maso, M., and Kulmala, M.: Production, growth and properties of ultrafine atmospheric aerosol particles in an urban environment, Atmos. Chem. Phys., 11, 1339–1353, https://doi.org/10.5194/acp-11-1339-2011, 2011.

Salma, I., Borsós, T., Németh, Z., Weidinger, T., Aalto, T., and Kulmala, M.: Comparative study of ultrafine atmospheric aerosol within a city, Atmos. Environ., 92, 154–161, https://doi.org/10.1016/j.atmosenv.2014.04.020, 2014.

Salma, I., Németh, Z., Weidinger, T., Kovács, B., and Kristóf, G.: Measurement, growth types and shrinkage of newly formed aerosol particles at an urban research platform, Atmos. Chem. Phys., 16, 7837–7851, https://doi.10.5194/acp-16-7837-2016, 2016.

Salma, I., Varga, V., and Németh, Z.: Quantification of an atmospheric nucleation and growth process as a single source of aerosol particles in a city, Atmos. Chem. Phys., 17, 15007–15017, https://doi.org/10.5194/acp-17-15007-2017, 2017.

Salma, I., Vasanits-Zsigrai, A., Machon, A., Varga, T., Major, I., Gergely, V., and Molnár, M.: Fossil fuel combustion, biomass burning and biogenic sources of fine carbonaceous aerosol in the Carpathian Basin, Atmos. Chem. Phys., 20, 4295–4312, https://doi.org/10.5194/acp-20-4295-2020, 2020a.

Salma, I., Vörösmarty, M., Gyöngyösi, A. Z., Thén, W., and Weidinger, T.: What can we learn about urban air quality with regard to the first outbreak of the COVID-19 pandemic? A case study from central Europe, Atmos. Chem. Phys., 20, 15725–15742, https://doi.org/10.5194/acp-20-15725-2020, 2020b.

Schmale, J., Henning, S., Henzing, B., Keskinen, H., Sellegri, K., Ovadnevaite, J., Bougiatioti, A., Kalivitis, N., Stavroulas, I., Jefferson, A., Park, M., Schlag, P., Kristensson, A., Iwamoto, Y., Pringle, K., Reddington, C., Aalto, P., Äijälä, M., Baltensperger, U., Bialek, J., Birmili, W., Bukowiecki, N., Ehn, M., Fjæraa, A. M., Fiebig, M., Frank, G., Fröhlich, R., Frumau, A., Furuya, M., Hammer, E., Heikkinen, L., Herrmann, E., Holzinger, R., Hyono, H., Kanakidou, M., Kiendler-Scharr, A., Kinouchi, K., Kos, G., Kulmala, M., Mihalopoulos, N., Motos, G., Nenes, A., O'Dowd, C., Paramonov, M., Petäjä, T., Picard, D., Poulain, L., Prévôt, A. S. H., Slowik, J., Sonntag, A., Swietlicki, E., Svenningsson, B., Tsurumaru, H., Wiedensohler, A., Wittbom, C., Ogren, J. A., Matsuki, A., Yum, S. S., Myhre, C. L., Carslaw, K., Stratmann, F., and Gysel, M.: Collocated observations of cloud condensation nuclei, particle size distributions, and chemical composition, Scient. Data, 4, 170003, https://doi.org/10.1038/sdata.2017.3, 2017.

Schmale, J., Henning, S., Decesari, S., Henzing, B., Keskinen, H., Sellegri, K., Ovadnevaite, J., Pöhlker, M. L., Brito, J., Bougiatioti, A., Kristensson, A., Kalivitis, N., Stavroulas, I., Carbone, S., Jefferson, A., Park, M., Schlag, P., Iwamoto, Y., Aalto, P., Äijälä, M., Bukowiecki, N., Ehn, M., Frank, G., Fröhlich, R., Frumau, A., Herrmann, E., Herrmann, H., Holzinger, R., Kos, G., Kulmala, M., Mihalopoulos, N., Nenes, A., O'Dowd, C., Petäjä, T., Picard, D., Pöhlker, C., Pöschl, U., Poulain, L., Prévôt, A. S. H., Swietlicki, E., Andreae, M. O., Artaxo, P., Wiedensohler, A., Ogren, J., Matsuki, A., Yum, S. S., Stratmann, F., Baltensperger, U., and Gysel, M.: Long-term cloud condensation nuclei number concentration, particle number size distribution and chemical composition measurements at regionally representative observatories, Atmos. Chem. Phys., 18, 2853–2881, https://doi.org/10.5194/acp-18-2853-2018, 2018.

Sihto, S.-L., Mikkilä, J., Vanhanen, J., Ehn, M., Liao, L., Lehtipalo, K., Aalto, P. P., Duplissy, J., Petäjä, T., Kerminen, V.-M., Boy, M., and Kulmala, M.: Seasonal variation of CCN concentrations and aerosol activation properties in boreal forest, Atmos. Chem. Phys., 11, 13269–13285, https://doi.org/10.5194/acp-11-13269-2011, 2011.

Sorjamaa, R., Svenningsson, B., Raatikainen, T., Henning, S., Bilde, M., and Laaksonen, A.: The role of surfactants in Köhler theory reconsidered, Atmos. Chem. Phys., 4, 2107–2117, https://doi.org/10.1007/978-0-306-48100-010.5194/acp-4-2107-2004, 2004.

873 Topping, D. O. and McFiggans, G.: Tight coupling of particle size, number and composition in atmospheric cloud droplet
874   activation, Atmos. Chem. Phys., 12, 3253–3260, https://doi.org/10.5194/acp-12-3253-2012, 2012.
875 Wex, H., McFiggans, G., Henning, S., and Stratmann, F.: Influence of the external mixing state of atmospheric aerosol on
876   derived CCN number concentrations, Geophys. Res. Lett., 37, 10805, https://doi.org/10.1029/2010GL043337, 2010.
877 Wiedensohler, A., Birmili, W., Nowak, A., Sonntag, A., Weinhold, K., Merkel, M., Wehner, B., Tuch, T., Pfeifer, S., Fiebig,
878   M., Fjäraa, A. M., Asmi, E., Sellegri, K., Depuy, R., Venzac, H., Villani, P., Laj, P., Aalto, P., Ogren, J. A., Swietlicki,
879   E., Williams, P., Roldin, P., Quincey, P., Hüglin, C., Fierz-Schmidhauser, R., Gysel, M., Weingartner, E., Riccobono, F.,
880   Santos, S., Grüning, C., Faloon, K., Beddows, D., Harrison, R., Monahan, C., Jennings, S. G., O'Dowd, C. D., Marinoni,
881   A., Horn, H.-G., Keck, L., Jiang, J., Scheckman, J., McMurry, P. H., Deng, Z., Zhao, C. S., Moerman, M., Henzing, B.,
882   de Leeuw, G., Löschau, G., and Bastian, S.: Mobility particle size spectrometers: harmonization of technical standards
883   and data structure to facilitate high quality long-term observations of atmospheric particle number size distributions,
884   Atmos. Meas. Tech., 5, 657–685, https://doi.org/10.5194/amt-5-657-2012, 2012.